Tectonophysics, 212 (1992) 351–370
Elsevier Science Publishers B.V., Amsterdam

The autocorrelation function: an image processing tool for fabric analysis

Renée Panozzo Heilbronner

Geologisch-Paläontologisches Institut, Universität Basel, Bernoullistrasse 32, CH-4056 Basel, Switzerland

(Received November 4, 1991; revised version accepted March 3, 1992)

ABSTRACT

Panozzo Heilbronner, R., 1992. The autocorrelation function: an image processing tool for fabric analysis. *Tectonophysics*, 212: 351–370.

The use of the autocorrelation function (ACF) is proposed as a method for fabric and/or strain analysis. Its chief purpose is to extend fabric analysis to fine-grained materials such as clays, micrites, etc., or to materials where the determination of individual grain shapes is tedious or impossible. The main advantage of the method is that no segmentation of the image prior to analysis is necessary; in other words, any bias associated with identifying grain boundaries and the like is avoided. In as much as the recognition of grains or grain boundaries is a matter of scale, the ACF can be used without loss of generality whenever the grain size is small in comparison with the size of the analysed area.

The method is computer-based: it requires a scanner for the digitization of the images and sufficient storage space and computing power for digital image processing. The method uses half-tone images as input. These can be obtained from thin sections, acetate peels, polished surfaces, photographic negatives or positives, etc.

The ACF is a two-dimensional function that is related to the average shape that occurs in the fabric. It is scaled with respect to the original image and allows simultaneous analysis of small and large features. The ACF enables: (a) a quantitative description of the fabric in general terms; (b) an efficient grain size determination; and (c) if strain is a valid interpretation of the fabric – the derivation of the finite strains in the plane of observation.

In the first part of the paper, the ACF method is introduced by way of a few numerically generated fabrics and compared to other methods of fabric and strain analysis. In the second part, an application to three samples of experimentally deformed Solnhofen limestone is demonstrated.

Introduction to the autocorrelation function

The mathematical definition of the autocorrelation function (ACF) shall be given very briefly, followed by a qualitative discussion of the function, which shall explain why the ACF can be used for fabric analysis. The method for calculating the ACF is given in the appendix. The less mathematically inclined reader may skip to the next section where a model for visualizing the ACF is offered.

In many textbooks on digital image analysis or digital image processing (e.g., Rosenfeld and Kak, 1976; Hall, 1979; Gonzalez and Wintz, 1987), the autocorrelation function (ACF) is introduced in the context of Fourier analysis and Fast Fourier Transforms (FFT). However, the ACF is perfectly well defined in object space, and although frequency considerations are sometimes very useful, the main reason for considering FFTs is the fact that they allow efficient calculation of the ACF. The ACF is defined by the following equation:

$$f(x,y) \otimes f(x,y) = \int_{-\infty}^{\infty}\int_{-\infty}^{\infty} f(x',y') \cdot f(x+x',y+y')\, dx'\, dy' \quad (1)$$

where $f(x,y)$ is the two-dimensional brightness function that defines the image, $\otimes$ is the opera-

Correspondence to: R. Heilbronner Panozzo, Geologisch-Paläontologisches Institut, Universität Basel, Bernoullistr. 32, CH-4056 Basel, Switzerland.

tor denoting a convolution or correlation, and x' and y' are the dummy variables of integration. Like the original image, the ACF is a two-dimensional function. Although the dimensions of the ACF and the original image are exactly the same, they have different meaning. In the original, a given coordinate point (x,y) denotes a position, whereas in the ACF, a given coordinate point (x',y') denotes the endpoint of a neighbourhood vector, and the value of the ACF at a given (x',y') denotes the correlation of *all* image points (x,y) with *all* neighbourhood points that are located at $(x+x',y+y')$.

The ACF describes how well an image correlates with itself under conditions where the image is displaced with respect to itself in all possible directions. Since a correlation (convolution) in object space "reduces" to a multiplication in frequency space, Fourier transforms may be used: the product of the Fourier transform of an image

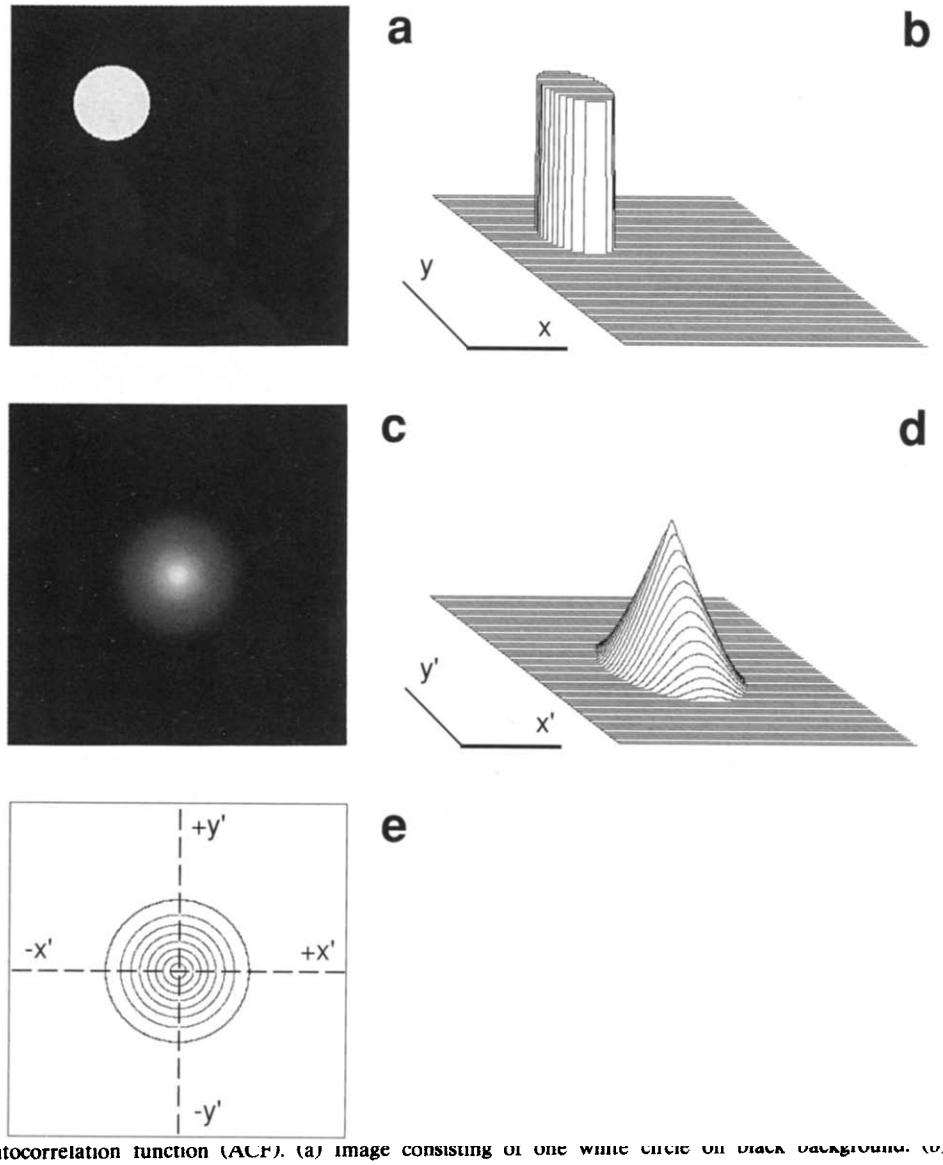

Fig. 1. The autocorrelation function (ACF). (a) Image consisting of one white circle on black background. (b) Perspective representation of the brightness function of the image. (c) Brightness representation of the ACF: zero displacement is at the center. (d) Perspective representation of the ACF. (e) Contour map of the ACF: contour levels are at 1, 32, 64, 96, 128, 160, 192, 224 (out of 256 grey values); origin is at the center.

times its complex conjugate is the Fourier transform of the ACF (see appendix). The most efficient way of calculating Fourier transforms is to use FFT methods (infact, without FFT algorithms, there would be no use in calculating the ACF in Fourier space).

Visualization of the ACF

The following model may help to understand the ACF. Let us imagine an image which consists of one white circle on a black background (Fig. 1a and b). Let us further imagine that two copies of this image are made on two overhead transparencies. The circles are completely transparent and the background is completely opaque. Holding the transparencies against a light source and superposing them, such that the circles coincide exactly, a state of maximum possible transmission of light is obtained. Starting at this position and keeping the first transparency fixed, the second film may be displaced in any direction. As it is shifted, the background area of the first film overlaps with the circle on the second film and vice versa. As a consequence, the total amount of transmitted light decreases. We may regard the amount of light that passes through both transparencies as a measure of the value of the ACF at that given displacement. By moving the second film through all possible x- and y-displacements while recording the amount of transmitted light, we obtain the brightness analogon of the ACF (Fig. 1c and d). The maximum of the ACF always occurs at zero displacement, irrespective of the position of the circle in the image. In this model, it is possible to shift one film entirely past the other, and thus, to obtain non-zero values for the ACF at distances that are as large or larger than the image size. However, this is an artefact, since the ACF is *not* sensitive to image size or shape. The ACF assumes that the image is a sample of a pattern that extends to infinity. We can model this by assuming infinitely large films.

For circles (or isotropic fabrics in general), the rate of decrease of the ACF values away from the origin is the same in all directions, thus the contour lines are circular (Fig. 1e). In cases were the fabric consists of ellipses or is otherwise anisotropic, the rate of decay of the ACF away from the center is not the same in all directions. The ACF remains high along directions parallel to the preferred orientation, i.e., in direction of long feature extension or low spatial frequencies; and it decreases rapidly in direction of short feature extensions or high spatial frequencies. As a result the contour lines of the ACF become elongated in the direction of maximum correlation. The relation between a given fabric and the shape of its ACF is the basis of the proposed new method of shape analysis

Practical application of the ACF

The standard application of the ACF is not in the field of image *analysis* but in the context of image *enhancement* or *restoration* (see, e.g., Fan and Cowley, 1985; Scandella et al., 1989). In these applications, the aim is not to extract a quantitative description of the geometry (such as, for example, two numbers signifying preferred orientation and average grain size), but to produce an improved version of the original image. Typically, the input image for such an application consists of a periodic pattern, and the resulting brightness representation of the ACF looks like a "cleaned-up" version of it. Geometry and symmetry of the unit cell are enhanced. However, as has been mentioned before, the result of the procedure is not a quantitative description, but instead, again, a full-size image.

In the field of image *analysis*, the ACF has not been used very extensively, and only limited investigations into the shape relation between original image and ACF have been carried out (e.g., Lins, 1984). A first description of the use of the ACF for geological fabric analysis has been made by the author (Panozzo Heilbronner and Gschwind, 1987). Optical data processing, i.e., the analysis of diffraction patterns, has been used by Pincus (1969a,b,c) to determine preferred orientations in relatively fine-grained fabrics. The digital equivalent of this method is the analysis of the power spectrum and the application of filter algorithms to enhance (or remove) certain preferred directions. However, diffraction patterns belong to Fourier space and any related tech-

nique focuses on the spatial frequency aspect of the image (and spatial frequency may be considered the inverse of shape). The ACF, on the other hand, is primarily developed in object space, i.e., it focuses directly on shape.

The main reason for applying the ACF analysis to fabrics is that it does not require segmentation (filtering, edge detection, contour chasing, etc.) of the images. In other words, there is no need to identify and trace grain boundaries or to fit ellipses or to find center points. This is particularly useful, when the fabric is very fine-grained, as in the case of micrites or shales, for example.

Carrying out an ACF analysis is a simple procedure. On the sample, a square region of appropriate magnification is selected, and digitized. This may be done in various ways. Either a scanner is attached to the microscope and the field of view is scanned directly, or another possibility is to first produce a photomicrograph of the area and to scan the negative or a photographic enlargement thereof. The image matrix may be preprocessed. In particular, one may desire to evaluate a sample area of a given fixed real size. Moreover, in order to make use of FFT algorithms, the image has to be tranformed to a square matrix of $2^n \times 2^n$ size, where n is an integer. The ACF is calculated as indicated in the appendix.

The *size* of the image has to be adapted to the size of the features one wishes to analyse. As has been mentioned, in the FFT calculation of the ACF, there is the implicit assumption that the image is a representative fraction of a pattern that extends infinitely in all directions. In the calculation this is realized by adding duplicates of the image on all four sides of the original. Thus, the edge of the image does not influence the shape of the ACF.

It is common practice to represent the ACF with the origin placed in the center. Since the ACF has a twofold symmetry it would, in principle, be sufficient to show only one half of it. However, it is much easier to evaluate symmetry and/or anisotropy if the complete ACF is shown. Generally, the width of the ACF peak comes out only a fraction of the input image. It is therefore useful to select and re-enlarge a central part of the ACF. If a given fabric is very fine-grained, the central peak of the ACF becomes very narrow. Technically, there is no problem in re-enlarging such peaks even if they are only a few pixels wide, however, the resulting contour lines become meaningless: they reflect much more of the square symmetry of the digitizing grid than the geometry of the fabric.

Thus, it is important to chose the initial magnification of the image such that a reasonable pixel resolution can be achieved. Good shape resolution and good sample statistics require opposing strategies: high magnification is chosen in order to resolve the shape of the ACF; low magnification is chosen in order to have as many grains on the area as possible (see appendix).

Interpretation of the ACF

The easiest way of evaluating the shape of the ACF contours is to use public domain image analysis software, such as, for example, "Image 1.25" by Rasband and Reeves (1988), and to measure size, axial ratio and orientation of the contours on appropriately thresholded brightness representations of the ACF.

When interpreting an ACF it is crucial to distinguish between physical and geometrical aspects, or rather, between objects and images. Our "problem" is that we see objects rather than images. The ACF, however, analyses images, not objects. Since the value of the ACF at a given displacement depends on the brightness distribution of the image, and since, in general, the grains are recognized on account of being areas of more or less constant brightness, it is likely that the brightness function of the total image depends most strongly on the contributions of the grains. However, there may still be other (larger or smaller) features that contribute significantly. These may relate to subregions (subgrains, grain boundary regions, etc.) or supraregions (aggregates of grains, ribbons, alignments, etc.). In other words, the ACF provides a simultaneous quantitative description of geometry at all scales of the image: from features that measure the equivalent of a few pixel, to those which measure up to a sizeable fraction of the image width.

In order to interprete the ACF of a given fabric, we have to make sure that we see the same image as that which the ACF "sees". We have to make sure that we recognize *all* fabric elements that contribute to the brightness distribution of the image, and thus, influence the final ACF. Let us assume, for example, that we wish to analyse a fabric where many grains show undulatory extinction in a direction oblique to the preferred orientation of the grains. The shape and orientation of the ACF contours depends on the shape and orientation of the coherent areas that represent the grains and on the orientation and intensity of the contrast edges that are the geometric expression of the undulatory extinction. Thus, the total ACF is a composite signal; it will not only reflect the average shape and the preferred orientation of the grains, but also the preferred orientation of the undulatory extinction. If we wish to analyse the grain shapes only, we have to find a lighting condition which suppresses the ondulous extinction. The ACF, of itself, is incapable of selecting the objects of interest.

Finally, it should be remembered that, while allowing the quantification of the *geometry* of a fabric, the ACF method does not automatically provide the analysis of the underlying *physical* phenomenon. In particular, crystallographic orientations can be analysed only in so far as they are expressed by a brightness contrast.

Autocorrelation functions of numerically generated fabrics

In order to demonstrate the application of the ACF analysis, a few numerically generated fabrics shall be discussed. The following symbols and definitions will be used:

r	radius of circle
a,b	long, short axis of ellipse
D	anticorrelating distance between center points
D_x, D_y	anticorrelating distance in x- and y-direction
d_{base}	diameter of base contour of ACF
d_{zero}	diameter of outer rim of zero area of ACF
$d_{1/2}$	diameter of ACF peak at one half peak height
$h(\alpha)$	orientation distribution function of long axes of ellipses
α_p	preferred orientation, mean of $h(\alpha)$
σ	standard deviation of $h(\alpha)$
$D \geqslant 4r$	diluted fabric
$2r < D < 4r$	dense fabric ($D < 2r$ would cause overlaps)
s	average intercept length of circles
S	average diameter of spheres

The first fabrics consist of sets of white circles on black background. In all cases, the center point distribution is random and anticlustered. The difference lies in the length of the anticorrelating distance, D, i.e., in the density of packing, and in the isotropy or anisotropy of the center point distribution. In fabric C1, the center point distribution is isotropic and the distance between center points is as large or larger than twice the radius of the circles: $D = 2r$ (Fig. 2a). Thus, the fabric is densely packed, circles may touch each other. In fabric C2, the center point distribution is isotropic and the anticorrelating distance is four times the radius of the circles: $D = 4r$ (Fig. 2b). Thus, the distance between the peripheries of the circles is at least as large as the diameter of one circle, the fabric is diluted. In fabric C3, the center point distribution is anisotropic, such that $D_x = 6r$ and $D_y = 3r$, where D_x and D_y are the anticorrelating distances in x- and y-direction respectively (Fig. 2c). The fabric is semi-diluted. Finally, in fabric C4 (Fig. 2d), the center point distribution is again anisotropic, $D_x = 4r$ and $D_y = 2r$, and the fabric is dense.

In the ACF, the central peak and the background correlation have to be considered in separate turns. As a first observation, the contour lines at the center of the ACFs of all fabrics are circular (Fig. 2e–h), indicating that at scale of the average grain size, the fabrics are isotropic.

In the case of the densely packed fabric, C1, the central peak grades into a low-level low-amplitude background correlation (Fig. 2e). In terms of the two-film model, this is explained by the following consideration: As soon as the two films are beginning to be displaced with respect to each other, such that the overlap of each circle

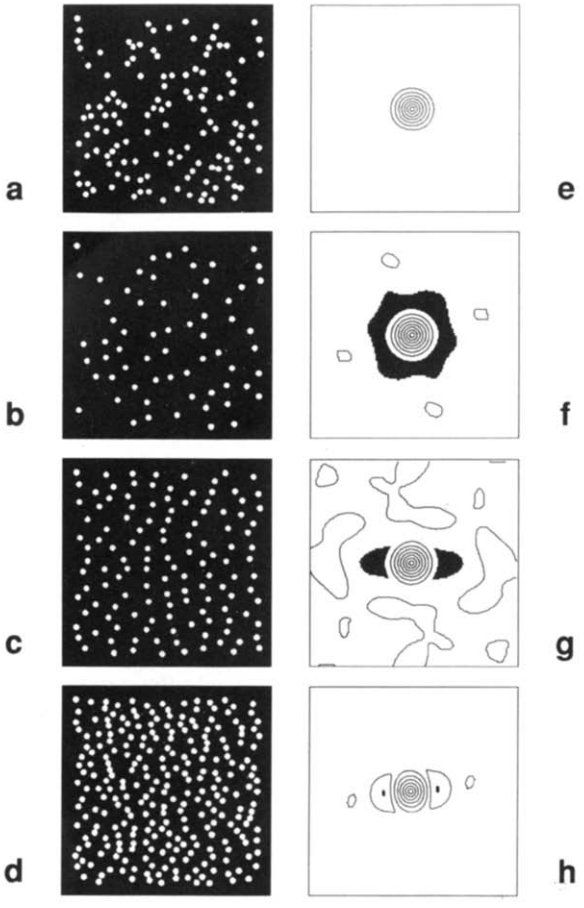

Fig. 2. Fabrics and ACFs of randomly distributed white circles of constant radius r. (a) Fabric C1: dense fabric of circles with random distribution of center points; anticorrelating distance $D = 2r$. (b) Fabric C2: diluted fabric of circles with isotropic random centerpoint distribution; anticorrelating distance $D = 4r$. (c) Fabric C3: semi-diluted fabric of circles with anisotropic random centerpoint distribution; $D_x = 6r$, $D_y = 3r$. (d) Fabric C4: dense fabric of circles with anisotropic random centerpoint distribution; $D_x = 4r$, $D_y = 2r$. (e) Contour plot of central window of ACF of (a). (f) Contour plot of central window of ACF of (b), black = zero area. (g) Contour plot of central window of ACF of (c), black = zero area. (h) Contour plot of central window of ACF of (d), black = zero area.

with itself decreases, new overlap areas among neighbouring circles begin to grow. Thus, rather than dropping to an absolute zero correlation, a mean average background with statistical fluctuations is attained. The regularity of the background depends on the packing density of the fabric and on the relative size of the distributed circles (and, in the case of numerically generated fabrics, on the quality of the random number generator).

Size relations

In the ACF of the diluted fabric C2 (Fig. 2b), a ring-shaped area of absolute zero (= zero area) occurs around the central peak (Fig. 2f). The inner rim is the base contour of the central peak, the diameter of which, d_{base}, is four times the radius of the circles:

$$d_{base} = 4r \tag{2}$$

Recalling the two-film model of the ACF again, it is obvious why this must be so. In diluted fabrics it is possible to attain a situation where all circles are completely blocked out by background area of the opposite film. This occurs whenever the relative shift is larger than the diameter of one circle, but small enough so that no overlaps between nearest neighbours can occur. In this situation, the ACF is zero. Decreasing the relative shift to $2r$, the circles begin to touch, and a first minimal correlation appears. In other words, if the zero area exists, the base contour of the ACF is exactly twice the diameter of the circles of the original image. If the fabric consists of randomly oriented shapes that are *not* circular, the diameter of the base contour is twice the *average* diameter of these shapes.

As a first approximation, the ACF peak is a cone. However, the slopes of the ACF profiles are not exactly linear as would be suggested by the triangular shape of the one-dimensional ACF of the rectangular function (Fig. 3a,b) (see, e.g., Gonzalez and Wintz, 1987). The two-dimensional ACF of a single circle has a fluted profile (Fig. 3c). For a set of circles which are arranged in a hexagonal close packing, the profile of the ACF is different again. Thus, considering profiles of the ACF that run through the origin, one notes that their exact shape depends on density and packing order of the fabric constituents.

Grain size determination through the ACF

In the one-dimensional case, the diameter of the ACF at one half peak height, $d_{1/2}$, is exactly

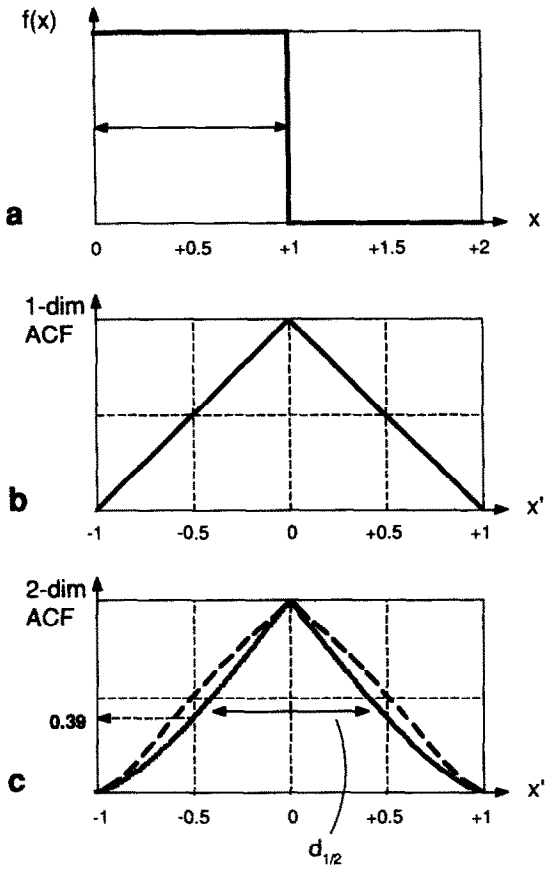

Fig. 3. One-dimensional and two-dimensional ACFs. (a) One-dimensional brightness function, representing a line of unit length (δ). (b) One-dimensional ACF of (a). (c) Solid line: central profile across two-dimensional ACF of unit one single circle of diameter δ; dashed line: centra across two-dimensional ACF of hexagonally close packed circles, along direction of closest packing.

the length of the original line (i.e., of the rectangular function). In the two-dimensional case of the single circle, $d_{1/2}$ is less than the diameter of the circle:

$$d_{1/2} = 0.81(2r) \tag{4}$$

and the contour for which the diameter is exactly equal to the diameter of the circle is at 0.39 of the maximum ACF (Fig. 3c). The profile in Figure 3c from which these two numbers are derived, has been obtained via a direct calculation of the ACF of a single circle, which is, in fact, equivalent to the calculation of the overlap area of two circles as they are moved apart. Note that $d_{1/2}$ of a single circle is very close to the average intercept length, s, of a circle, which is given as:

$$s = 0.78(2r) \tag{4}$$

where $(2r)$ is the average diameter of the circle. This relation is the same as the relation between the average diameter of sectional circles and the average diameter of the original spheres. The statistics of the frequency distribution of sectional circles and that of the population of spheres from which the circles are generated have been studied by Monte Carlo methods (Panozzo, 1982). It can be shown that the average diameter of sectional circles is always 0.78 times the average diameter of the spheres, and from this one can infer that the average intercept length of circles is always 0.78 times the average diameter $(2r)$ of the circles; only the standard error depends on the number of measurements and on sorting.

In the case of closely packed circles, $d_{1/2}$ in direction of closest packing is exactly equal to the diameter of the circles. One would expect that the ACF of statistically packed circles — representing a fabric which is "denser" than that consisting of one circle but less dense than a fabric of hexagonally closest packing — has a profile shape somewhere inbetween the first two:

$$0.81(2r) \leqslant d_{1/2} \leqslant 2r \tag{5}$$

In practical applications it has been found that $d_{1/2}$ is often very close to the single circle case, such that one can assume that $(2r) \approx (1/0.81)d_{1/2} \approx 1.2d_{1/2}$.

For three-dimensional extrapolations, by the argument given above, the average diameter of the circles, $(2r)$, has to be multiplied by $1/0.78$ $(= 1.28)$ in order to obtain the average diameter, S, of spheres from which the circles have been obtained (Panozzo, 1982). Thus, assuming that $(2r)$ is usually close to 1.2 $d_{1/2}$, one finds:

$$S = 1.28 \times 1.2d_{1/2} \approx 1.5d_{1/2} \tag{6}$$

All the above considerations rest on the assumption that the thickness of thin sections is much smaller than the average grain size. Obviously, for very fine-grained material this is not necessarily true. In these cases, one should either use ultra-thin sections, polished surfaces or ac-

etate peels, or the derived grain size has to be corrected via stereological correction formulae. Underwood has compiled various methods for estimating grain size from projection images (Underwood, 1970); it appears that corrections are necessary only if $t/S \gg 1$, i.e., if the ratio between section thickness and average grain diameter exceeds unity (see, p. 185ff.). These correction formulae are calculated for images where opaque and spatially dispersed particles are projected onto the image plane. However, the grains of a crystalline fabric are usually transparent and closely packed. Although this situation is conceptually different, the prediction, that corrections are necessary only if $t/S > 1$, has been verified in many practical applications. Projecting several layers of transparent grains onto the image plane creates a visual texture of a given graininess. Once the ratio of $t/S > 1$, the grain size of this texture and the corresponding ACF grain size begin to decrease. Thus, if thin sections of very fine-grained materials are analysed (i.e., if $t/S \gg 1$), the relationship between the grain size of the visual texture and that of the projected grains has to be assessed independently. Note, however, that the *shape* of the ACF is usually not affected by section thickness.

Autocorrelation and anticorrelation

Returning to the considerations of the zero area, we may observe an interesting relation between the ACF method and Fry's method (1979). The outer rim of a zero area (such as shown in Fig. 2f) is exactly equivalent to the outer rim of the "empty space" in the anticorrelation diagrams described by Fry. From the film model it is obvious that the outer radius of the zero area must be $D - 2r$. Hence, the diameter of the outer rim of the zero area, d_{zero}, is given by:

$$d_{zero} = 2D - 4r \qquad (7)$$

If $D \gg 4r$ (as in the case of the ideal center-point plot) $d_{zero} = 2D$. In other words, if the ACF method is applied to center point plots, Fry's analysis is exactly duplicated.

If the center point distribution is anisotropic, such as in fabrics C3 and C4, equation (7) has to be generalized in order to take into consideration the dependence of d_{zero} on direction. If D_x and D_y are the anticorrelation distances and $d_{zero}(x)$ and $d_{zero}(y)$ the diameter of the outer rim in the x- and y-directions respectively, the axial ratio, $d_{zero}(y)/d_{zero}(x)$, of the outer contour is $(D_y - 4r)/(D_x - 4r)$. If $D_x \gg 4r$ and $D_y \gg 4r$, this reduces to D_y/D_x.

In the case of fabric C3, dilution is only partly sufficient, and while $D_x = 4r$, $D_y < 4r$. In this case, the outer rim of the zero area recedes below the base contour of the central peak (Fig. 2g). Still, the anisotropic shape of the zero area (which is not contiguous anymore) can be recognized. In fabric C4, dilution is completely insufficient, and only small remnants of the zero area can be seen (Fig. 2h). Moreover, a ridge of higher correlation is created parallel to the direction of highest center point density, creating central contour lines that are elongated in direction of shortest anticorrelating distance. This seeming contradiction again demonstrates that Fry's method is fully contained in the ACF analysis. In fact, Fry's method can be interpreted as the ACF method applied to a small subclass of images, namely those images which are derived from center point plots. While Fry's method is restricted to the *auto*correlation analysis of spatially *anti*correlated, and dimensionless, center points, the method proposed here considers the *auto*correlation of any image. The fabrics discussed here, C1 to C4, consist of spatially anticorrelated, but *extended*, "center points", i.e. circles.

Description of isotropy and anisotropy of fabrics

We will now turn to the ACF of anisotropic shapes, and consider five fabrics that consist of ellipses. The center point distribution of these fabrics is random, anticorrelated and isotropic, the fabrics are densely packed, the anticorrelating distance D is $2a$ (Fig. 4). Fabrics E1, E2, E4 and E5 have been created using a random number generator, fabric E3 is the strained version of an isotropic fabric like E1. Size and axial ratio is the same for all ellipses, the axial ratio, b/a, is 0.50. In fabric E5, a second set of ellipses of half

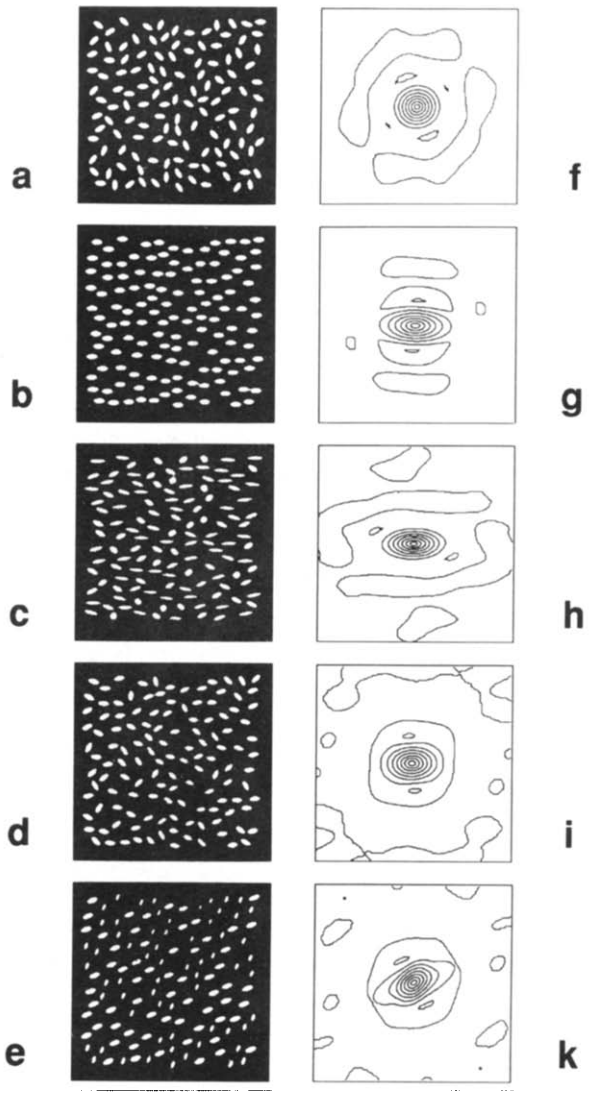

Fig. 4. Fabrics and ACFs of randomly distributed ellipses. (a), (f) Fabric E1: randomly oriented ellipses. (b), (g) Fabric E2: parallel ellipses. (c), (h) Fabric E3: strained version of randomly oriented ellipses: b/a of strain ellipse = 0.5, $R_s = 2.00$. (d), (i) Fabric E4: ellipses with preferred orientation $\alpha_p = 0° \pm 30°$. (e), (k) Fabric E5: two sets of ellipses parallel to two preferred orientations; $a_2 = (1/\sqrt{2})a_1$; $\alpha_{p1} = 20°$ and $\alpha_{p2} = 70°$.

the size is present. In the strained fabric, E3, $2a$ and b/a must vary as a function of orientation.

Fabric E1, while consisting of anisotropic shapes, is isotropic because of the random orientation of ellipse long axes (Fig. 4a and f). This is reflected in the ACF contours which are circular at the center (minor deviations and structure of background correlation are due to the random number generator that was used to create the fabrics). The background ACF of this and all other fabrics, except E3, portrays the isotropy of the center point distribution. This is a somewhat unnatural situation because one would expect that the centerpoint distribution of sedimentary or crystalline fabrics is influenced by the anisotropy of the particles of which it is composed.

Fabric E2 is anisotropic, consisting of perfectly parallel ellipses (Fig. 4b and g). The central ACF contours of this fabric are elliptical and parallel, the axial ratio is 0.5. That the axial ratio of the ACF contours is exactly identical to that of the ellipses is easily understood if we picture a set of diluted parallel ellipses (where $D > 4a$). Using the film model for visualization, and generalizing equation (2), we derive that the base contour is exactly twice the size of the fabric ellipses: $d_{base}(x\text{-direction}) = 4a$ and $d_{base}(y\text{-direction}) = 4b$, thus, the axial ratio of the contour is b/a.

For fabric E1 and E2, the ACF contours yield the same axial ratio as would be obtained from the application of the SURFOR and the PAROR method (Panozzo, 1983, 1984). It also coincides with the characteristic shape of the SURFOR analysis (see appendix Schmid et al., 1987). All three methods provide a measure of global isotropy or anisotropy, the difference being that the ACF and PAROR method consider areas (i.e., volumes) whereas the SURFOR analysis considers only outlines (i.e., surfaces). Thus, the axial ratio, b/a, and orientation, ϕ, derived from the ACF contours is a measure for the axial ratio and the preferred orientation of the fabric anisotropy.

Strain determinations

Fabric E3 is obtained by straining a fabric like E1: the axial ratio of the applied strain is 0.5 (strain ratio $R_s = 2.0$) and the maximum elongation is in horizontal direction (Fig. 4c and h). The ACF contours are elliptical, again, b/a is 0.5. Note that, here, the background correlation is anisotropic too.

For the following consideration of fabrics E1, E2 and E3, we may disregard the contour lines of the background ACF, or we may assume that they are identical to the central contours (since

we could easily produce fabric E2 with an anisotropic center point distribution). On the basis of the ellipticity of the peak contours, we may interpret these three fabrics in terms of strain; E1 appears unstrained ($R_s = 1$) and for E2 and E3, the inferred strain ratio is $R_s = 2$. If the ACFs of two fabrics, such as E2 and E3, are identical, it means that, on the *average*, the fabrics are identical too. This is not in contradiction to the fact that they may differ with respect to size, axial ratio and orientation of their *individual* components. In order to discriminate such fabrics, a method like the R_f-ϕ technique (Ramsay, 1967) has to be used. The R_f-ϕ plots of E2 and E3 are different. However, the inferred strain, i.e. the average anisotropy which is related to strain, is the same. The ACF is a statistical method which cannot recognize individual features. It can discriminate *average* large and small features. If we consider an ACF contour of one given size, it does not relate to *one* ellipse in the original, rather it relates to *all* possible neighbourhoods of that size.

General description of preferred orientations

Fabric E4 consists of ellipses with a preferred orientation, α_p, of long axes (Fig. 4d and i). The orientation distribution function $h(\alpha)$ is defined by the Gaussian normal distribution:

$$h(\alpha) = \frac{1}{\sqrt{2\pi\sigma}} \exp\left[(\alpha_p - \alpha)^2 / 2\sigma^2\right] \qquad (8)$$

where α is the angle of orientation of the long axis of an ellipse, α_p is the mean and σ the standard deviation of the orientation distribution. The ACF contours are elongated, but most are not elliptical. The axial ratio of the contour lines, b/a, is 0.66. This ratio is identical to that obtained from the PAROR analysis of the fabric (Panozzo, 1983), which, in turn, is derived from the convolution of the orientation distribution of the long axes of ellipses times the projection function, $h(\alpha) \otimes s(\alpha)$. A preferred orientation of anisotropic shapes (with $\sigma(\alpha) \neq 0$) produces a fabric which is less anisotropic than the average individual shape. If the orientation distribution function of the long axes, $h(\alpha)$, is symmetric, the resulting fabric is orthorhombic. As long as the fabric is orthorhombic, deviations from ellipticity are not easy to recognize. In the particular case discussed here, we have an a priori knowledge that the ACF should deviate from ellipticity: we know that the fabric is generated by a normal distribution of long axes, and there is the notion that the "average shape" of normally distributed ellipses is not necessarily an ellipse. Compare Wheeler's (1988) and DePaor and Kusky's (1988) discussions on the "guitar shaped" envelope of pebbles.

In principle, it is possible to regard the distinction between elliptical and non-elliptical contours (whether orthorhombic or of even lower symmetry) as a criterion for the discrimination of strained fabrics from others. But, as has been pointed out, in applications to natural samples, this distinction is generally quite difficult. The only distinction that can be made in practice, is one between elliptical (or orthorhombic) and non-orthorhombic (i.e., monoclinic or "asymmetric") ACF contours.

Fabrics of less than orthorhombic symmetry

Fabric E5 consists of two sets of ellipses, which have a bimodal orientation distribution function. The axial ratio of the ellipses is 0.50 in both cases. The larger set is oriented at 20° and is of the same size as in the previous fabrics, the smaller set is half the size and is oriented at 70°. As the preferred orientations, α_{p1} and α_{p2} of the two sets of ellipses are not 90° apart, the resulting ACF contours, particularly those at the lower peak levels, are of lower than orthorhombic symmetry (Fig. 4e and k). Moreover, the contours are not geometrically similar at all peak levels. (The two-fold symmetry, inherent to the ACF is, of course, still present).

At this point, the shape relation between ACF contours and image geometry needs to be reconsidered. So far, we have treated it as one of geometric similarity, but this is not generally valid. Let us consider the fabrics shown in Figure 5a and b. They consist of randomly dispersed rectangles and rhombs. The center point distribution is isotropic anticlustered with an anticorrelating distance $D = 4a$. As a consequence, complete or

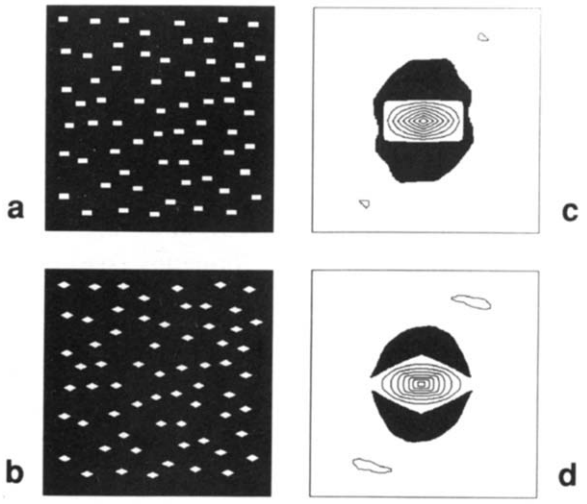

Fig. 5. ACFs of non-elliptical, orthorhombic shapes. (a) Randomly distributed, parallel rectangles. (b) Randomly distributed, parallel rhombs. (c) ACF of (a), black = zero area. (d) ACF of (b), black = zero area.

nearly complete zero areas are formed. The base contours are rectangular or rhombic (Fig. 5c and d). Using the film model we can understand why this is so.

As the ACF rises from the base contour to the peak, rhombs are converted to rectangles and vice versa. We now have to leave the simple concept of geometric similarity used so far, and adopt the concept of self-correlation in its own right. The rhombic contour lines of the ACF of the rectangles indicate high correlation in direction parallel to the sides of the rectangles. Again, this can be understood if we consider the film model: at short displacements the overlap of rectangles remains largest if the shift is parallel to the sides of the rectangles and not diagonally as would be needed to obtain rectangular ACF contours. For rhombs, an analogous "inverse" shape relation may be observed: the rectangular ACF contours at higher levels indicate high correlation parallel to the sides of the rhombs, i.e., parallel to the diagonal of the resulting rectangular ACF contours.

Note, however, that the axial ratios and diameters derived from the ACF contours are still correct. Moreover, the fact that the shape relation between ACF and image seems to be "inverse" does not invalidate what has been observed for elliptical fabrics so far. It only highlights the special symmetry of ellipses. Unlike other orthorhombic shapes, the ellipse is invariant with respect to the "shape inversion" of the ACF.

In all cases where ACF contours deviate from ellipticity, probably the most profitable way of using the ACF is to re-examine the original fabric, after one has obtained an information about its symmetry through the ACF. "Interesting" looking ACF contours can be used to detect "interesting" objects or neighbourhoods in the original image. In a very general way, one evaluates directions of high correlation, which may indicate preferred orientations *or* alignments *or* elongated shapes, which in turn can be due to grain boundaries, subgrains, grain clusters or other structures.

In terms of size relations one can use two possible links between ACF and image: (a) the base contour, if it exists, and (b) the empirical size relation given by equation (5). Proceeding from the ACF to the image, one could take a contour between 0.39 and 0.50 of the ACF peak height (see section on grain size determination) and try to find the average object of that size. If that contour is very non-elliptical, an object of "inverse" shape must be sought. The alternative is to proceed from the image (and maybe some a priori knowledge of it), and to first establish the average size of the objects of interest, and then to evaluate the ACF contour of the corresponding size. The general experience with various methods of fabric analysis is that they teach us to see. Shapes or symmetries that were not recognized previously, not even suspected to exist, often become quite obvious after they were brought out by the analysis.

Criteria for the sense of rotation

With respect to the shape of ACF contours, two aspects of symmetry may be distinguished: (a) the symmetry of the individual contour shapes, i.e., whether they are orthorhombic or less than orthorhombic; and (b) the orientational relation among contours of different levels of the ACF, i.e., whether they are parallel or rotated with respect to one another.

The lozenge shape of the contours of fabric E5 (Fig. 4e and k) (which are not identical but "inversely related" to the lozenge shapes that are often observed in shear zones) permit the definition of two independent criteria for sense of rotation.

(1) The *center-out criterion*: The orientation of long axes drawn to the ACF contours is considered. The rotation needed to align the long axes of the higher level contours with those of the lower level contours, i.e., the rotation necessary to align small features with large features, is called the center-out criterion.

(2) The *second-to-first criterion*: The shape of ACF contours of less than orthorhombic symmetry (usually below $\frac{1}{2}$ peak height) is considered. The main preferred orientation is in direction of the apex of the contours, a secondary direction is defined by a "hump" situated at less than 90° with respect to the first. The rotation needed to align the secondary with the primary preferred orientation is termed the second-to-first criterion.

According to both criteria, the fabric E5 has a dextral sense of rotation. A detailed discussion of rotational "asymmetries" is outside the scope of this paper. It may suffice here to assert that (a) such low symmetry ACFs are quite common in natural samples, and (b), that the rotation criteria are mutually independent, since fabrics have been observed where the sense of rotation inferred from center-out and second-to-first coincide, and others, where they are in contradiction. There are many ways in which low ACF symmetries can be explained. In the context of deformed materials, this may be by non-pervasive deformation mechanisms such as migration and alignment of grain or subgrain boundaries, or by processes that lead to strain partitioning such as subgrain rotation advancing the rotation of grains, etc. In the context of such explanations, oblique ACF contours may by used as indicators of sense of shear.

Comparison between ACF analysis and other methods

Summarizing a comparison made between the ACF analysis presented here, the R_f-ϕ method (Ramsay, 1967), the PAROR and SURFOR methods (Panozzo, 1983, 1984), and the anticorrelation method introduced by (Fry, 1979), the following can be noted:

(a) *Global and local fabrics*: The ACF and Fry's anticorrelation analysis are global methods. In other words, they are not useful for extracting information about individual features. The fabric is considered as a whole, information concerning local anisotropy is averaged. In contrast, the R_f-ϕ, SURFOR and PAROR methods, while providing a global analysis, retain some local information: in the R_f-ϕ scatter plots or in the rose diagrams of surface or long axis orientations, information about local anisotropies is recorded.

(b) *Correlation*: Since Fry's method evaluates the correlation among anticorrelated center points, it can be considered a special case of the ACF method. The ACF and the anticorrelation diagrams coincide perfectly, if the extension of the components, i.e. the center points, is negligeable with respect to the anticorrelating distance(s).

(c) *Bias*: The amount of bias introduced by the various methods differs widely. The R_f-ϕ and anticorrelation methods require intensive "preprocessing" of data: fitting ellipses to particles in one case, finding center points in the other. The PAROR and SURFOR methods require segmentation of the image and contour tracing. Only the ACF analysis requires no preprocessing at all. The disadvantage of this is, of course, that features which are not part of the fabric (such as dust, stains, etc.) will also influence the result of the analysis.

(d) *Scale*: The ACF method has the advantage of simultaneously quantifying the fabric geometry at all scales of the image (which, depending on image size, is between one and two decades), each contour relating to image features of corresponding size. It therefore yields a more complete analysis than any of the other methods of fabric analysis.

(e) *Consistency*: Although the ACF is based on an entirely different concept, it yields results that are entirely consistent with those obtained from the other methods (R_f-ϕ method, Fry's method, SURFOR and PAROR methods). This will be borne out further by the following section.

(f) *Elliptical shapes and strain*: With a sensitivity similar to that of the rose diagram of the SURFOR method, the ACF is capable of detecting deviations from orthorhombic symmetry. Therefore, the shape of the ACF contours may be used as a strain test: If all contours of a given ACF are circular or elliptical and parallel, the fabric may be interpreted in terms of homogeneous strain. The axial ratio and orientation of the ACF contours are directly related to the strain ellipse. If the contour lines are not orthorhombic, strain interpretations have to be excluded.

(g) *Non-elliptical shapes*: Shapes that deviate from ellipticity may still be symmetric (e.g., squares, rectangles, rhombs, etc.). The shape relation between ACF contours and shapes of fabric components ceases to be one of geometrical similarity. Still, the axial ratio of the fabric anisotropy is the same as that determined by PAROR or SURFOR methods.

(h) *Low symmetry*: If the shapes of the ACF contours are of lower than orthorhombic symmetry, two mutually independent senses of rotation may be determined. This is similar to the shear sense inferred from the rose diagram or the characteristic shape of the SURFOR analysis.

Application of the ACF analysis to real fabrics

In order to discuss the application of ACF analysis to real fabrics, three samples of experimentally deformed Solnhofen limestone shall be considered. The samples are taken from a work by Schmid et al. (1987). Solnhofen limestone is very fine-grained, having an average grain size of 4–5 μm. Even on ultra thin sections (section thickness $\leqslant 5$ μm), only the shape of the very largest grains can be resolved clearly. The analysis presented in the above mentioned paper made use of the PAROR and SURFOR method and was based on manually digitized contours of the largest grains in a section. The authors assumed that no strain partitioning between large and fine grains had occurred, and that, accordingly, the fabric determined from the largest grains would be identical to the bulk fabric. The samples that were selected for the comparison between ACF and PAROR/SURFOR methods are ST2, ST1 and

TABLE 1

Results of fabric analysis of experimentally deformed Solnhofen limestone by SURFOR and PAROR method (samples from Schmid et al., 1987)

	(1)	(2)	(3)	(4)	(5)	(6)	(7)	(8)
			Theory		SURFOR		PAROR	
	T (°C)	γ	b/a	ϕ (°)	b/a	ϕ (°)	b/a	ϕ (°)
ST2	500	1.22	0.32	29	0.36	31	0.32	30
ST1	700	1.07	0.36	31	0.57	33	0.54	32
ST4	900	1.36	0.28	28	0.85	– *	0.84	– *

(1) T temperature of experiment
(2) γ applied shear strain
(3–4) theoretical values, calculated for applied displacement
(3) b/a axial ratio of finite strain ellipse ($1/R_s$)
(4) ϕ orientation of long axis of finite strain ellipse, measured anticlockwise from positive x-axis
(5–6) values derived from SURFOR analysis
(5) b/a axial ratio of surface fabric
(6) ϕ preferred orientation of surface, measured anticlockwise from positive x-axis
(7-8) values derived from PAROR analysis
(7) b/a axial ratio of particle fabric
(8) ϕ preferred orientation of particles, measured anticlockwise from positive x-axis

* not defined due to large axial ratio b/a.

ST4, which were deformed at 500°C, 700°C and 900°C respectively (see Table 1).

The intended comparison involves two steps: (1) the ACF analysis is applied to the very same drawings that formed the basis for the published PAROR and SURFOR analyses (Fig. 6a–c), and (2) the ACF is applied to newly scanned areas of the same sites in the ultra thin sections (Fig. 7a–c). In the first step, the question is: how closely does the ACF analysis reproduce the results of the SURFOR and PAROR method? In the second step, the question is: Is the bulk fabric of Solnhofen limestone really the same as the fabric of the largest grains?

Test 1: Is the ACF analysis consistent with other methods?

The digitized outlines are converted to black and white matrices. Each area enclosed by an outline is white, the background is black, as shown in Figure 6a–c. The ACF of these images is shown in Figure 6d–f. The values for the axial ratio, b/a, and the orientation, ϕ, of the ACF contours are compiled in Table 2.

A spectrum of fabrics, from strong flattening (ST2, deformed at 500°C) to almost isotropic (ST4, deformed at 900°C) can be observed. From the PAROR analysis the average long diameter of the grain contours is easily obtained; as a consequence, there is no problem in selecting the appropriate contour level of the ACF: it is 128 (i.e., at half peak height) for all samples (see Table 2). The average long diameter indicated in column (1) is the average of the largest grains; it is not the true average, which should be much smaller.

For ST2, the axial ratio obtained from the ACF is 0.04 below the PAROR value; the orientation is the same. For ST1, the axial ratio obtained from the ACF is 0.06 below the PAROR value, the orientation is within one degree of the PAROR orientation. For ST4, the axial ratio obtained from the ACF is 0.05 higher than the value obtained from PAROR analysis. Due to the weak anisotropy, the orientation could not be determined with any reasonable security. Thus, the results obtained from ACF analysis are within ± 0.05 of the b/a value obtained from the PAROR method. Note, that this amount of deviation is of the same order of magnitude as the discrepancies between PAROR and SURFOR results (compare columns 5 and 7 of Table 1 and column 3 of Table 2).

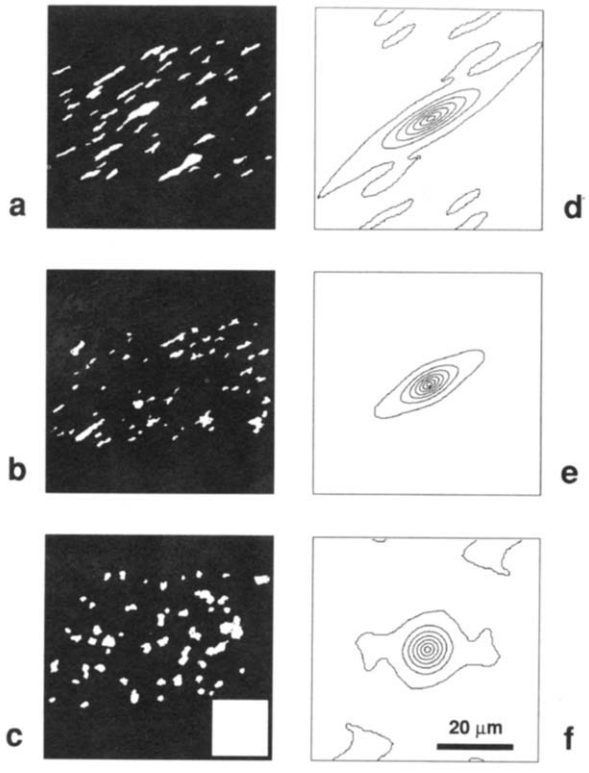

Fig. 6. ACF analysis of experimentally deformed Solnhofen limestone. (a–c) Images which are obtained from manual digitization of grain boundary contours (true image width is 240 μm). (d-f) ACFs which are magnified 4:1 with respect to the original images. White inset on (c) shows the relative size of the ACFs. (a) and (d) ST2 (500°C); (b) and (e) ST1 (700°C); (c) and (f) ST4 (900°C).

Comparing results of PAROR, SURFOR and ACF analysis, it is impossible to say which of the methods yields the "true" result. Each of the three methods refers to a different aspect: SURFOR to the orientation of the contour lines, PAROR to shape *and* orientation of the enclosed areas, and the ACF to shape, orientation and distribution of the areas in the x-y plane. However, it may be argued that the most appropriate comparison is one between the ACF and the PAROR, because both relate to areas, not to outlines.

The PAROR method considers the projection of shapes, thus, it does not consider the shape itself but an equivalent shape which is produced by drawing an envelope around each shape. The shapes considered by the ACF are more "skeletal" and of smaller local diameter than the shapes considered by the PAROR method. Thus, if the shapes are convex–concave the axial ratio, b/a, obtained from the ACF may be expected to be somewhat smaller than the value derived from the PAROR method, as is the case for ST2 and ST1. If the grains are more convex, the results may coincide better. Note also, that if the grains are closely packed, the skeletal nature of the individual grains is less important, since there is always a neighbouring grain protruding into a concave embayment, inhibiting a drastic decrease of the ACF function value in that direction.

In summary, the comparison demonstrates that the ACF results are perfectly equivalent to PAROR results, and, in cases where PAROR and SURFOR results are the same, ACF analysis is also equivalent to SURFOR analysis. In as much as different aspects of the fabrics are analysed, the results are different. For "well-behaved" fabrics, however, the derived values may be expected within 5% for b/a, and within 1 or 2 degrees for ϕ.

Test 2: Is the large-grain fabric the same as the bulk fabric?

For the evaluation of the bulk fabric, areas of Solnhofen limestone were scanned under bright field illumination and parallel polarizers (Fig. 7a–c). The corresponding ACFs are shown in Figure 7d–f. The width of each field is approximately 100 μm. While the structural situation (centre of shear zone) of the samples could be reproduced, the exact location could not be found. Again, a transition from strong anisotropy (elongated grains) to an almost isotropic fabric (equant grain shape) is obvious. Again, for the derivation of the axial ratio, those ACF contours were picked which correspond to a measured grain size of the fabric. In this case (where an independent grain size measurement was not available), an average starting grain size of 4 to 5 μm was assumed. The measured axial ratio and a slight grain growth was taken into consideration. In all cases, the contours at one quarter of the peak height come out to be the most appropriate ones. The b/a and ϕ values obtained for these contours also are listed in Table 2. The fact that the contour corresponding to the average grain size is at such a low level of the ACF peak indicates that the grain

TABLE 2

ACF analysis of experimentally deformed Solnhofen limestone (samples from Schmid et al., 1987).

	(1)	(2)	(3)	(4)	(5)	(6)	(7)
	Diameter b/w plot	ACF of contour lines			ACF of halftone image		
		Diameter contour	b/a	ϕ (°)	Diameter contour	b/a	ϕ (°)
ST2	15.6	14.8	0.28	30	4.5	0.39	33
ST1	8.6	8.1	0.48	31	5.1	0.55	29
ST4	8.9	7.6	0.88	– *	5.6	0.88	– *

(1) average long diameter (μm) of outlines used for SURFOR and PAROR analysis (Schmid et al., 1987)
(2–4) ACF analysis of hand-made tracing of contour lines
(2) true length of long diameter (μm) of ACF contour, contour level is at 0.5 of peak height
(3) axial ratio of ACF contour
(4) preferred orientation of ACF contour, measured anticlockwise from positive x-axis
(5–7) ACF analysis of image as scanned from thin section
(5) true length of long diameter (μm) of ACF contour, contour level is at 0.25 of peak height
(6) axial ratio of ACF contour
(7) preferred orientation of ACF contour, measured anticlockwise from positive x-axis

* not defined due to large axial ratio b/a.

size of the visual texture, i.e., the "grain size" that would be inferred from the contour at approximately half the peak height, is smaller and probably stems from projection effects (grain overlap) and substructures (such as relief contrast), but not from the actual, physical calcite grains.

In view of the deviations that are already to be expected among the results of the SURFOR and PAROR analysis (see above discussion), the comparison between the ACF analysis of the bulk rock and the ACF analysis of large grains must be judged a very good one (compare column 6 and 3 of Table 2). That is, one may safely conclude that the large-grain fabric and the bulk fabric are the same.

Discussion

That the small difference in b/a value between large-grain fabrics and bulk fabrics could be explained by a certain sampling variance has

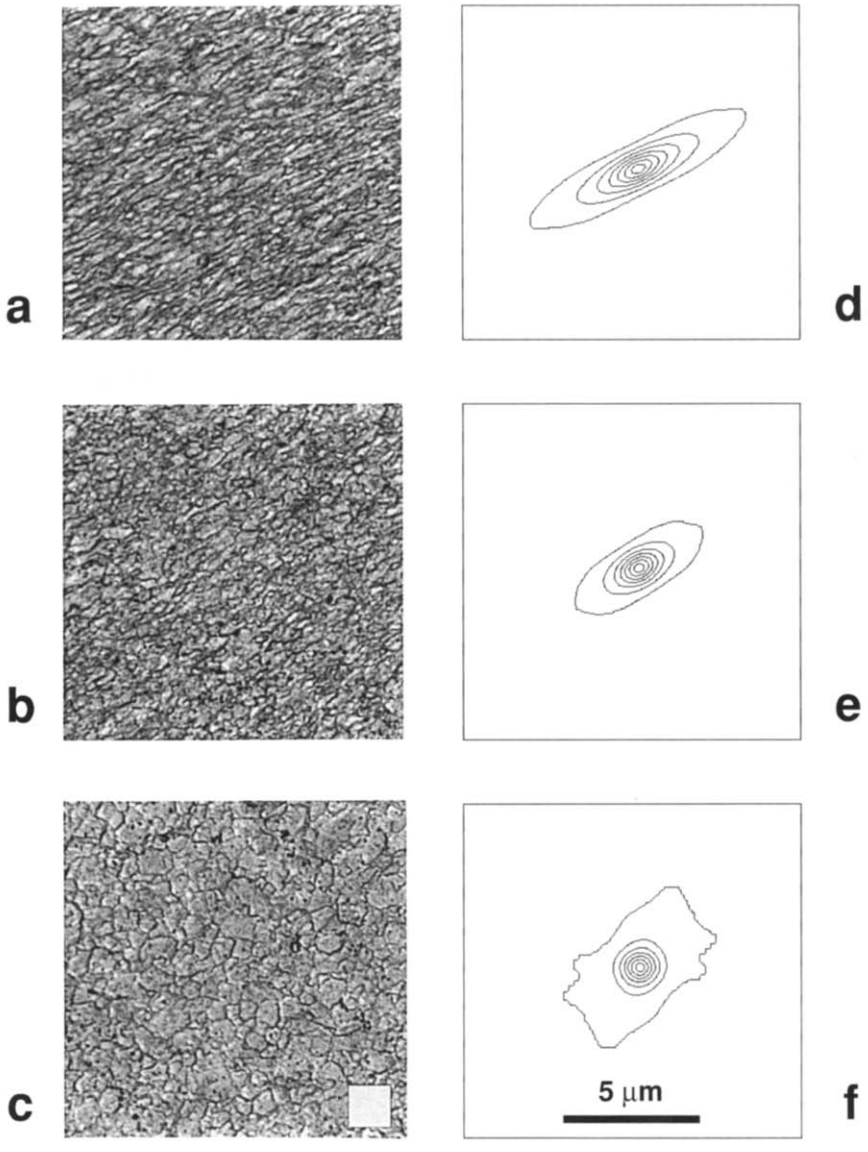

Fig. 7. ACF analysis of experimentally deformed Solnhofen limestone. (a-c) Images which are obtained by scanning thin sections under parallel polarizer conditions (true image width is 100 μm). (d–f) ACFs which are magnified 8 : 1 with respect to the original images. White inset on (c) shows the relative size of the ACFs. (a) and (d) ST2 (500°C); (b) and (e) ST1 (700°C); (c) and (f) ST4 (900°C).

been indicated above. Another explanation can be found if the geometric similarity among the contours is reconsidered (Fig. 7d–f). One finds that the b/a ratio is higher at higher levels and lower at lower levels, indicating stronger anisotropy for larger objects or "neighbourhoods" than for smaller ones. This dependence of ACF contour shape on peak level is most pronounced in the case of ST2, less so in the case of ST1 and more or less absent in the case of ST4 (excluding the lowest contour line which already grades into the background correlation).

Since ST2 and ST1 were deformed in the intracrystalline slip regime, one might envisage strain partitioning as an explanation for such differences in large and small scale fabrics. (ST4 was deformed in the grain boundary sliding regime, and strain considerations must be excluded.) Another explanation would be that, at higher temperatures, *one* (self-identical) fabric tends to pervade the sample at all scales, whereas, at the lower temperatures, there seems to be an increasing decoupling of large and small scale deformation. (For the image size discussed here, "all scales" means a little more than one decade). In any case, the assertion that the bulk fabric is identical to the fabric of the larger grains, has to be modified: *On the average*, i.e., at the scale of the average grain size, the bulk fabric does coincide with the fabric of the large grains, but the degree of penetration of this fabric to smaller sizes is a function of temperature.

In all samples, the background correlation does not fluctuate much, no secondary maxima are obvious. The lowest contour of the ACF peak is interesting. By its size it describes the correlation at a scale of two to four average grain diameters, thus, it may refer to the larger grains analysed previously. In the case of ST2, the axial ratio and orientation derived from the lowest contour is closer to the respective PAROR values (which were derived from larger grains). And these values in turn are identical to the applied strain (see Table 1). For ST1, the lowest contour also has a smaller b/a ratio than the higher level contours. In fact, the lowest contour value is lower than the PAROR value, and represents a closer match to the applied shear strain. Is it possible then, that the lowest contour is sensitive to a "ghost" of a strain marker in spite of the fact that the deformation of the fabric occurred under *P-T* conditions, which normally obliterate most or all of the original grain boundaries? In a study on experimentally sheared calcite gouge, another type of ghost structures has been described (Friedman and Higgs, 1981). These structures consist of stringers of impurities, the orientation of which closely tracks the direction of the finite strain ellipse. In contrast, in the case discussed here, the physical nature of the "ghosts" is not clear; they are not impurities. Moreover, they seem to record not only the orientation but also the axial ratio of the finite strain ellipse. The lowest contour of ST4 is clearly non-elliptical, only the direction of its longest extension indicates a dextral shear sense.

Summary and conclusions

In this paper, the ACF has been introduced in order to provide a quantitative description of fabric geometry, of grain size and, within certain limits, of strain. The ACF is intended for fabric interpretation not for classification.

The ACF method has the following applications:

(1) Grain size measurements: from an ACF contour at a level between 0.39 and 0.50 of the total peak height, the average grain size can be inferred.

(2) The ACF yields anticorrelation diagrams (Fry, 1979) if center point plots are used as input images.

(3) The ACF yields the axial ratio, b/a, and orientation ϕ of the surface fabric anisotropy in cases where the dominant brightness elements of the digitized fabric are surfaces and grain boundary regions.

(4) The ACF yields the axial ratio, b/a, and orientation ϕ of the particle fabric anisotropy in cases where the dominant brightness elements of the digitized fabric are cross sectional areas of particles.

(5) The ACF provides a means to test whether a fabric is compatible with an interpretation in terms of strain. If the contour lines are elliptical and parallel, the fabric may be interpreted in

terms of strain. If the contour lines are non-elliptical (at least not orthorhombic), a strain interpretation is more or less impossible.

(6) The ACF provides two independent criteria for the determination of a sense of rotation.

(7) The ACF provides simultaneous analysis at all scales of the image (for 512×512 image size, this is usually a little more than one decade).

Thus, the ACF method is a valid and efficient method, which yields results that are consistent with those derived from other methods of fabric or strain analysis. The method is fast and unbiased because no segmentation of the image prior to analysis is necessary. Most of the time used for the the derivation of the ACF is spent on data acquisition. On the equipment used here, a 512×512 matrix is scanned in 20 minutes (including calibrations), the calculation of the ACF and the preparation of the contour plot is a matter of seconds.

Acknowledgements

This work has profited from a very fruitful collaboration with Ruedi Gschwind (Departement of Scientific Photography, University of Basel), from financial support by the Swiss National Science Foundation (NF Grant 2.162-0.83), from critical comments by Holger Stünitz (Geological Institute, University of Basel), and constructive reviews by D.G. DePaor, G.J. Borradaile and M. Friedman.

Appendix: Calculation of the autocorrelation function using the Fast Fourier Transform (FFT)

Use of FFT algorithms requires that the image be given as a two-dimensional complex function, the real and imaginary part relating to the amplitude and phase information, respectively. For the purpose of calculating the ACF, however, the phase information may be neglected, and only the real part of the function needs to be considered. In order to still benefit from the advantages of FFT methods, we simply convert this function to a complex one and set the imaginary part to zero. A further requirement for the application of the FFT algorithms is that the width of the image matrix be an integer power of 2, for example $2^9 = 512$. It is thus most convenient to use square images.

The sample area should be at least 20 particles wide, and, on the average, particles should be at least 10 to 20 pixels wide. Therefore, matrix size should be at least 256×256. For reasons that are explained in the text, a grain size of 10 to 20 pixels produces ACF peak contours which are 20 to 40 pixels wide. Taking an image of 512×512, and re-enlarging a central window of 128×128 of the ACF to the original size (which yields a four-fold magnification with respect to the image), contour lines have a diameter of 80 to 160 pixels. This allows good evaluation of the shape of contours, and at the same time, a sizeable portion of the background correlation can be examined.

The following procedure for calculating the ACF is used:

(a) The digitized image matrix is read into a complex array. The imaginary part is set to zero. For a 512×512 matrix this requires 2 Mbyte memory space.

(b) The mean brightness is calculated and subtracted.

(c) The two-dimensional discrete Fourier transform is given by:

$$F(U,V) = \frac{1}{N} \sum_{X=0}^{N-1} \sum_{Y=0}^{N-1} F(X,Y) \cdot \exp[-2\pi i(UX+VY)/N] \qquad \text{(A1)}$$

where $F(X,Y)$ is the discrete brightness function, X and Y are the discrete image coordinates, $N = 2^m$ (where m is an integer) is the size of the matrix, and i is $\sqrt{-1}$. $F(U,V)$ is the discrete transform, and U and V are the frequencies in x- and y- direction.

(d) The transform is calculated using the theorem of separability, which says that:

$$F(U,V) = \frac{1}{N} \sum_{X=0}^{N-1} F(X,V) \cdot \exp[-2\pi i(UX)/N] \qquad \text{(A2)}$$

where:

$$F(X,V) = \sum_{Y=0}^{N-1} F(X,Y) \cdot \exp[-2\pi i(VY)/N] \qquad \text{(A3)}$$

In other words, two consecutive one-dimensional FFTs are used to transform the rows and columns of the image matrix.

(e) Following the correlation theorem:

$$f(x,y) \cdot F(x,y) \Leftrightarrow F^*(u,v) \cdot F(u,v) \qquad \text{(A4)}$$

the Fourier transform of the ACF is obtained by multiplying the Fourier transform of the image, $F(u,v)$, with its complex conjugate $F^*(u,v)$.

(f) The inverse transformation is applied. Since:

$$F(X,Y) = \frac{1}{N} \sum_{U=0}^{N-1} \sum_{V=0}^{N-1} F(U,V) \cdot \exp[-2\pi i(UX+VY)/N] \qquad \text{(A5)}$$

i.e., since forward and backward transformation are essentially the same, rows and columns of the transform are back-transformed via two consecutive one-dimensional FFTs too, just as described in step (d) of the forward transformation. Throughout the calculation, one (complex) array is used. One after the other, it contains the original image, then the Fourier transforms and finally the resulting ACF. Since the mean value has been subtracted, the first value of the ACF array should be zero. As a second check, the imaginary parts of the ACF should be zero too.

(g) Finally, the ACF is stored as a byte array. The real parts of the complex ACF array are scaled and transformed to 8-bit integers such that the maximum and minimum values correspond to 255 (= white) and 0 (= black) respectively.

An extensive treatment of Fourier transformations and FFT applications in digital image processing is given by, e.g., Brigham (1974) or Gonzalez and Wintz (1987). The calculations were performed on a Microvax 3200, the programs were written in FORTRAN, and the FFT algorithm was imported from the IMSL Library (1987). This is the simplest program that could be obtained with minimal programming time. There are various ways in which it should be optimized, in particular, by making use of the conjugate symmetry of the transforms.

Rasband and Reeves have released a new version of their public domain program, "Image 1.28", which is capable of performing ACF calculations.

It is not necessary to preprocess the input images in order to obtain uniform image quality. Since the brightness function $f(x,y)$ of the image is real, and provided the ACF is normalized, as described above, the ACF is invariant with respect to linear point operations (i.e., with respect to image transformations where the new pixel value depends only on the old pixel value but not on the values of its neighbours). In other words, the ACFs of the positive, negative or the equalized version of an image are exactly the same. Note, however, that, in general, the effect of crossed polarizers cannot be considered a point operation, since the relative extent of bright and dark areas may vary as the thin section is rotated between polarizers.

References

Brigham, E.O., 1974. The Fast Fourier Transform. Prentice-Hall, Englewood Cliffs, N.J. 252 pp.

DePaor, D.G. and Kusky, T.M., 1988. Strain analysis in rocks with pretectonic fabrics: discussion. J. Struct. Geol., 10: 529–530.

Fan, G.Y. and Cowley, J.M., 1985. Auto-correlation analysis of high resolution electron micrographs of near-amorphous thin films. Ultramicroscopy, 17: 345–356.

Friedman, M. and Higgs, N.C., 1981. Calcite fabrics in experimental shear zones. Am. Geophys. Union, Geophys. Monogr., 24: 11–27.

Fry, N., 1979. Random point distribution and strain measurements. Tectonophysics, 60: 89–105.

Gonzalez, R.C. and Wintz, P., 1987. Digital Image Processing, 2nd edition. Addison-Wesley, Reading, Mass.

Hall, E.L., 1979. Computer Image Processing and Recognition. Academic Press, New York, N.Y., 584 pp.

IMSL MATH/LIBRARY, Version 1.0, April 1987. IMSL, Customer Relations, Houston, Texas.

Lins, N., 1984. Textural image processing on granular structures of metal shadowing replicas. Ultramicroscopy, 12: 185–200.

Panozzo, R., 1982. Determination of size distributions of spheres from size distributions of circular sections by Monte Carlo methods. Microscopica Acta, 86: 37–48.

Panozzo, R., 1983. Two-dimensional analysis of shape fabric using projections of digitized lines in a plane. Tectonophysics, 95: 279–294.

Panozzo, R., 1984. Two-dimensional strain from the orientation of lines in a plane. J. Struct. Geol., 6: 215–221.

Panozzo Heilbronner, R. and Gschwind, R., 1987. Bias and distortion in high resolution strain analysis. G05.63P, EUG IV, 13–16 April, Strassbourg.

Pincus, H.J., 1969a. Sensitivity of optical data processing to changes in rock fabric. Part I-geometric patterns. Int. J. Rock Mech. Min. Sci., 6: 259–268.

Pincus, H.J., 1969b. Sensitivity of optical data processing to changes in rock fabric. Part II-standardized grain patterns. Int. J. Rock Mech. Min. Sci., 6: 269–272.

Pincus, H.J., 1969c. Sensitivity of optical data processing to changes in rock fabric. Part III-rock fabrics. Int. J. Rock Mech. Min. Sci., 6: 273–276.

Ramsay, J.G., 1967. Folding and Fracturing of Rocks. MacGraw-Hill, New York, N.Y.

Rasband, W. and Reeves A., 1988. Image 1.25. National Institute of Health, Research Services Branch NIMH.

Rosenfeld, A. and Kak, A.C., 1976. Digital Image Processing. Academic Press, New York, N.Y., 457 pp.

Scandella, L., Anselmetti, D., Eng, L., Hidber, H.R., Jung, T., Meyer, E., Lapka, R., Staufer, U., Wiesendanger, R., Güntherodth, H.-J., Gschwind, R. and Heilbronner, R., 1989. Statistical method applied to STM measurements on ordered and disordered systems. Conf. STM 1988, Oxford.

Schmid, S.M., Panozzo R. and Bauer, S., 1987. Simple shear experiments on calcite rocks: rheology and microfabric. J. Struct. Geol., 9: 747–778.

Underwood, E., 1970. Quantitative Stereology. Addison-Wesley Publishing Company, Reading, Mass.

Wheeler, J., 1988. Strain analysis in rocks with pretectonic fabrics: reply. J. Struct. Geol., 10: 531–532.